Vertical coupling between short range surface plasmon polariton mode and dielectric waveguide mode

Ruiyuan Wan, Fang Liu,[a] Xuan Tang, Yidong Huang, and Jiangde Peng
Department of Electronic Engineering, State Key Lab of Integrated Optoelectronics, Tsinghua University, Beijing 100084, China

(Received 10 November 2008; accepted 23 February 2009; published online 7 April 2009)

Coupling performance between a short range surface plasmon polariton (SRSPP) mode and a conventional dielectric waveguide mode is demonstrated numerically. Simulation results show that the coupling length, as short as tens of microns, can be realized because the field of SRSPP extremely concentrates to the metal surface. SRSPP-based hybrid coupler provides not only an approach to realize highly compact functional devices, such as the TE-pass polarizer with high performance, but also an integratable route for efficiently exciting SRSPP mode, which is very useful in the SRSPP-based biosensor or SRSPP-assisted emission enhancement devices. © *2009 American Institute of Physics*. [DOI: 10.1063/1.3111001]

Surface plasmon polariton (SPP) is a transverse-magnetic surface electromagnetic excitation that propagates along an interface between metal and dielectric medium.[1] For a thin metal film embedded in dielectrics, the SPPs on the upper and lower metal-dielectric interfaces couple and form a symmetric mode and an asymmetric mode.[2] The symmetric mode with field extending into the dielectrics has comparatively lower loss and is referred to as long range SPP (LRSPP).[2] The metal strip guided SPP modes had been studied[3] and various LRSPP-based optical devices had been shown.[4,5] However, the asymmetric mode, referred to as short range SPP (SRSPP) mode, receives less attention than the LRSPP mode due to its much higher propagation loss and unclear applications. Besides, for the SRSPP mode, the π phase difference between the field on the two metal film surfaces makes it nearly impossible to be excited with present integratable method.[6]

Recently, it was reported that the SRSPP mode is promising for the biosensor to detect the refractive index change in ultrathin layer with high sensitivity[7] and the enhancement in internal quantum efficiency of silicon nanocrystals.[8,9] Therefore an integratable excitation method for the SRSPP mode is required for its further applications. Our group has proposed the hybrid coupler structure and demonstrated the high efficient coupling between the LRSPP mode and the dielectric waveguide mode.[10,11] In this paper, based on a vertical hybrid coupler structure, it is theoretically demonstrated that the SRSPP mode also can be excited by using the coupling property with the conventional single dielectric waveguide mode. This not only provides an efficient route for exciting SRSPP mode within a rather short length, which is very useful for the integratable SRSPP biosensor of ultrathin layer detection and the light sources with SRSPP-assisted emission enhancement structure, but also makes it possible to realize some highly compact functional devices, such as the TE-pass polarizer with much shorter length, high extinction ratio (ER), and comparatively low insertion loss (IL) due to the characteristics of the SRSPP mode.

Figure 1 shows the proposed vertical hybrid coupler. The two arms have different width, W_m and W_d, and different film thicknesses, T_m and T_d, to get similar effective index for high efficient coupling. D stands for the separation between the two arms. Coupling occurs only for TM mode because SRSPP is TM polarized. Here, we assume that the Au ($\varepsilon_m = -132 + i \times 12.65$) strip is surrounded by SiO_2($n_s = 1.444$) at $\lambda = 1.55$ μm, with fixed thickness of $T_m = 15$ nm and width of $W_m = 2$ μm. SiN_x($n_d = 2$) (Ref. 12) waveguide is chosen for the dielectric arm with $T_d = 220$ nm and $W_d = 1$ μm.

The proposed coupler has two bounded TM polarized eigenmodes, mode A and B, which were calculated by using software FEMLAB.[13] Their complex amplitudes of x-directional magnetic fields (H_x) are shown in Fig. 2, where $D = 1.2$ μm. Figures 2(a) and 2(c) show the 2–dimentional mode pattern of real part of H_x for mode A and B, respectively. The corresponding line profiles of field distribution across the center of two arms are also illustrated. It can be seen from both the 2D mode pattern and line profiles of field that the field surrounding the upper Au arm is antisymmetric distribution, which clearly shows the modal property of SRSPP. The eigenmode A and B arise from the in-phase and opposite-phase coupling between SRSPP and dielectric waveguide mode, respectively.

Different from the LRSPP-based coupler,[10,11,14] in the case of the SRSPP, the imaginary part of the field can be comparable with the real part and should be taken into account. This is for the reason that the SRSPP mode, with field much more concentrated to the metal strip, has comparatively high loss. Figures 2(b) and 2(d) show the imaginary

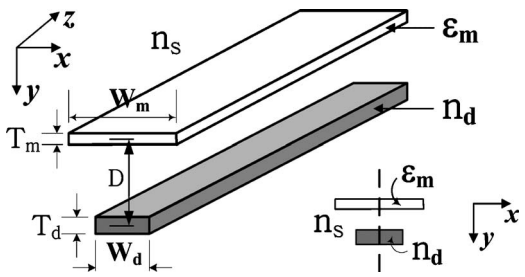

FIG. 1. Vertical hybrid coupler, white arm (upper) stands for metal strip and dark arm (lower) stands for dielectric waveguide. The right lower inset shows the x-y plane cross-section of the hybrid coupler and the dashed line crosses the center of two arms.

[a]Electronic mail: liu_fang@mail.tsinghua.edu.cn.

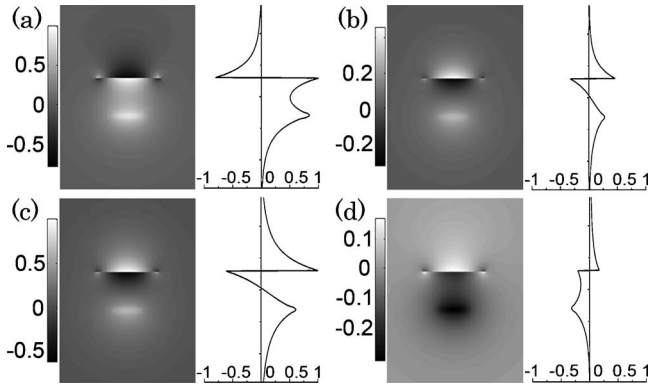

FIG. 2. Complex amplitudes of H_x of two TM eigenmodes in x-y plane. (a) and (b) shows real and imaginary part of mode A. (c) and (d) shows real and imaginary part of mode B. The line profiles are corresponding 1D field distribution along the dashed line shown in inset of Fig. 1.

part of mode A and B, respectively. By comparing (b) and (c), it can be seen that the imaginary part of mode A looks like the real part of mode B, but with smaller magnitude.

With above eigenmodes, any TM mode supported by the hybrid coupler can be expressed as follows:

$$\mathbf{H}(x,y,z) = a_{\mathrm{A}} e^{-\beta_{\mathrm{A}i} z} \mathbf{H}_{\mathrm{A}}(x,y) e^{-i\beta_{\mathrm{A}r} z} + a_{\mathrm{B}} e^{-\beta_{\mathrm{B}i} z} \mathbf{H}_{\mathrm{B}}(x,y) e^{-i\beta_{\mathrm{B}r} z}. \quad (1)$$

Here, $\mathbf{H}_{\mathrm{A}}$ and $\mathbf{H}_{\mathrm{B}}$ are the complex magnetic fields of eigenmodes A and B ($z=0$), respectively, and $\beta_{\mathrm{A}}=\beta_{\mathrm{A}r}-i\times\beta_{\mathrm{A}i}$ and $\beta_{\mathrm{B}}=\beta_{\mathrm{B}r}-i\times\beta_{\mathrm{B}i}$ are the corresponding complex propagation constants. Both of them can be calculated by software FEMLAB. At the input end, the incident field $\mathbf{H}_d$ ($\mathbf{E}_d$) of individual dielectric (lower) arm is considered as a single TM mode, then the corresponding mode coupling complex coefficients a_{A} and a_{B} can be derived from

$$a_m = \frac{1}{2}\int (\mathbf{E}_d \times \mathbf{H}_m)\hat{z}dA = |a_m| e^{i\theta_m} \quad (m = \mathrm{A},\mathrm{B}). \quad (2)$$

According to the unconjugated version of Eq. (11-16) in Ref. 15, all the modes are normalized and orthonormalized. Where $|a_m|$ and θ_m represent the magnitude of amplitude and coupling initial phase of corresponding eigenmode, respectively. Different from low-loss modes, here the phase part of the coupling coefficient θ_m is no longer just 0 or π, which results in complex initial amplitude of the eigenmode a_m. According to Eq. (1), the intensity of the magnetic field supported by the coupler can be expressed as

$$|\mathbf{H}(x,y,z)|^2 = \sum_m b_m^2 |\mathbf{H}_m(x,y)|^2 + 2b_{\mathrm{A}}b_{\mathrm{B}}\mathrm{Re}\{\mathbf{H}_{\mathrm{A}}(x,y)\mathbf{H}_{\mathrm{B}}^*(x,y)e^{-i\Delta\beta z}\},$$

$$(b_m = a_m e^{-\beta_{mi} z},\ m = \mathrm{A},\mathrm{B},\ \Delta\beta = \beta_{\mathrm{A}r} - \beta_{\mathrm{B}r}). \quad (3)$$

According to Eq. (3), we can depict how energy couples from the lower arm to the upper arm. Figure 3 shows the intensity of the magnetic field along z direction and the real part of H_x at the coupling distance $z=L_c$. It is clearly shown that the TM mode in the lower dielectric arm transfers gradually to the SRSPP mode in the upper metal arm. This coupling characteristic provides not only a method to excite SRSPP mode, but also an approach to realize highly compact

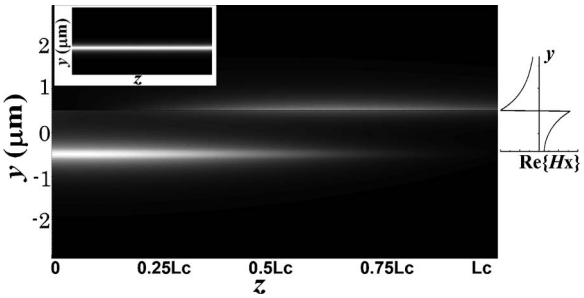

FIG. 3. Intensity of TM polarized magnetic field (sampled along dashed line in the inset of Fig. 1) as a function of propagation length z when $D=1$ μm. The left upper inset shows the TE mode directly passing through the dielectric arm. The line profile is the real part of H_x at the coupling distance $z=L_c$.

functional devices. At the coupling distance $z=L_c[L_c=\pi/(\beta_{\mathrm{A}r}-\beta_{\mathrm{B}r})]$, Eq. (3) can be simplified as

$$|\mathbf{H}(x,y,L_c)|^2 = |b_{\mathrm{A}}\mathbf{H}_{\mathrm{A}}(x,y) - b_{\mathrm{B}}\mathbf{H}_{\mathrm{B}}(x,y)|^2. \quad (4)$$

According to the field pattern in Fig. 2, Eq. (4) indicates that most of the energy has been coupled to the upper Au arm when $z=L_c$.

The effective indices of the eigenmode A and B and the coupling length L_c are shown in the inset of Fig. 4, as a function of D. It can be seen that L_c of SRSPP coupler could be diminished to less than 25 μm, which is about 1/10 of LRSPP-based coupler.[10,14]

It can be noticed from Fig. 3 that output power from the upper metal arm is lower than the input power because of the high loss of mode A and B, demonstrated by attenuation constant β_i/k_0 (Fig. 4). When $D<1$ μm, the coupling length L_c is relatively short [19–31 μm when $D=0.7-1$ μm (inset of Fig. 4)]. In this case, the transmission loss within L_c is comparatively low (1.1–4.4 dB when $D=0.7-1$ μm). While when $D>1.2$ μm, the coupling becomes weak and L_c increases dramatically, which results in high transmission loss over 10 dB. Therefore, compared with LRSPP-based coupler, high efficient coupling should be operated under much smaller D due to the tightly bounded SRSPP mode. Both smaller arm separation and shorter coupling length are significant for realizing highly compact optical components. Here, we ignore the coupling between LRSPP mode and dielectric waveguide mode because the significantly large effective index difference between LRSPP mode and SRSPP mode supported by thin metal strip[3] makes

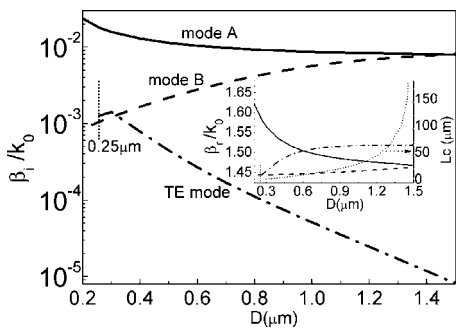

FIG. 4. Attenuation constants (β_i/k_0) of mode A (solid curve), mode B (dashed curve), and TE mode (dot-dashed curve) vs arm separation D. Inset shows corresponding effective index of each mode as well as coupling length (dotted curve).

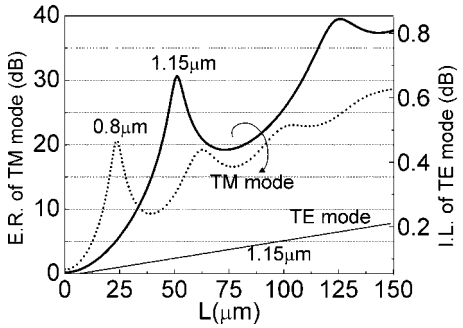

FIG. 5. ER curve of TM mode vs length L of proposed polarizer, labeled with $D=0.8$ μm (dotted) and 1.15 μm (thick solid). Also, the insert loss of TE mode when $D=1.15$ μm is shown as the thin solid line.

it difficult to get effective coupling for LRSPP mode to dielectric waveguide which has been designed to couple with the SRSPP mode.

Coupling characteristics between the two arms of the hybrid coupler discussed above is just for TM mode. For the TE mode guided by dielectric arm, no coupling can occur. The influence of Au arm can be ignored for relatively large D, while when D becomes smaller, the influence of Au arm gets noticeable. In the region of $D<0.6$ μm, the attenuation of TE mode increases and the effective index decreases dramatically, and the cutoff distance is found at $D=0.25$ μm (Fig. 4).

According to the coupling and loss characteristics analyzed above, a compact polarizer can be realized. Let us consider that TE and TM modes are input into the dielectric arm simultaneously, the TE mode will pass directly through the dielectric arm (inset of Fig. 3), while the TM mode will be filtered rapidly within a very short transmission length due to the coupling between two arms. Therefore, high TM ER and low TE IL can be realized.

At the output end $z=L$, coupling coefficient between the coupled mode and individual dielectric waveguide TM mode $\mathbf{H}_d$ ($\mathbf{E}_d$) is

$$a_L = \frac{1}{2}\int [\mathbf{E}_d \times \mathbf{H}(x,y,L)]\hat{z}dA$$

$$= \sum_m |a_m|^2 e^{-\beta_{mi}L} e^{i(2\theta_m - \beta_{mr}L)}, \quad (m = \mathrm{A,B}). \tag{5}$$

Therefore the total loss of TM mode is determined by $-20\ \lg(|a_L|)$. For TE mode, the similar formula could be deduced. Here loss of TM mode approximately represents the ER, and that of the TE mode represents the IL.[16]

Using Eq. (5), the ER of TM mode with $D=0.8$ and 1.15 μm as a function of the coupler length L were calculated, respectively (Fig. 5). It can be seen that the ER curve of TM mode increases rapidly along L with a strong ripple. The ripple indicates the coupling between the dielectric mode and SRSPP mode or the interference of eigenmodes A and B. The peak corresponds to the position where the TM mode transforms almost to the SRSPP mode. The period of the beat is in close agreement with $2L_c$. However, as seen in Eq. (2) and (5), the difference in the phase of complex coupling coefficients ($\Delta\theta=\theta_A-\theta_B$) resulting in nonzero couple-induced phase difference between two eigenmodes. Therefore the position of first peak appears at $z=(\pi+2\Delta\theta)/(\beta_{Ar}-\beta_{Br})$, which is a little longer than L_c.

Compared with conventional SPP-based TE-pass waveguide polarizer,[16,17] the proposed polarizer can have shorter device length, high ER, and comparatively low TE IL. Since the SRSPP mode has much higher loss than general SPP modes, the ER for TM mode increases rapidly along L. In addition, due to the concentrated field of SRSPP mode, small arm separation D can be adopted to achieve extremely short coupling length. It is noticeable in Fig. 5 that the ER is high up to 20 and 30 dB at the first peak position when $D=0.8$ and 1.15 μm, with the transmission length is only about 25 and 50 μm, respectively. Benefit from such short device length, the IL of TE mode can be comparatively low. Take $D=1.15$ μm, for example, the IL of TE mode is only about 0.1 dB when $L=50$ μm (Fig. 5). Therefore, TE-pass polarizer with high performance and rather short length could be realized. Furthermore, it is estimated that device size can be further reduced with thinner metal thickness, since increased loss for TM mode caused by more concentrated field of SRSPP mode make it easier to obtain high ER in shorter length, so long as we decreased D to maintain the strong coupling.

In conclusion, we demonstrate numerically the high efficient coupling between SRSPP mode and conventional dielectric waveguide TM mode. The proposed coupler has rather compact size because the field of SRSPP extremely concentrates to the metal surface. Simulation results show that the length of SRSPP-based coupler can be as short as tens of microns. This provides not only an approach to realize highly compact functional devices, such as the TE-pass polarizer with much shorter length, high ER, and comparatively low IL, but also an integratable route for efficiently exciting SRSPP mode, which solves the bottleneck for the SRSPP-based integratable biosensor and SRSPP-assisted emission enhancement devices.

This work is supported by the 973 Program of China under Contract No. 2007CB307004. The authors would like to thank Professor Wei Zhang, Xue Feng, and Yi Rao, as well as Mr. D. Ohnishi, H. Takatsu, and A. Kamisawa of ROHM Corporation for their helpful comments.

[1] H. Raether, *Surface Plasmons* (Springer, Berlin, 1988), pp. 4–13.
[2] J. J. Burke and G. I. Stegeman, Phys. Rev. B **33**, 5186 (1986).
[3] P. Berini, Phys. Rev. B **61**, 10484 (2000).
[4] T. Nikolajsen, K. Leosson, and I. Bozhevolnyi, Appl. Phys. Lett. **85**, 5833 (2004).
[5] R. Charbonneau, C. Scales, I. Breukelaar, S. Fafard, N. Lahoud, G. Mattiussi, and P. Berini, J. Lightwave Technol. **24**, 477 (2006).
[6] R. Charbonneau, P. Berini, E. Berolo, and E. Lisicka, Opt. Lett. **25**, 844 (2000).
[7] J. T. Hastings, Opt. Express **15**, 17661 (2007).
[8] X. Hu, Y. Huang, W. Zhang, and J. Peng, Appl. Phys. Lett. **89**, 081112 (2006).
[9] X. Tang, Y. Huang, Y. Wang, W. Zhang, and J. Peng, Appl. Phys. Lett. **92**, 251116 (2008).
[10] F. Liu, Y. Rao, Y. Huang, W. Zhang, and J. Peng, Appl. Phys. Lett. **90**, 141101 (2007).
[11] F. Liu, Y. Rao, X. Tang, R. Wan, Y. Huang, W. Zhang, and J. Peng, Appl. Phys. Lett. **90**, 241120 (2007).
[12] M. M. Tilleman, D. Haronian, and D. Abraham, J. Microlithogr., Microfabr., Microsyst. **5**, 023011 (2006).
[13] COMSOL AB, FEMLAB RF module model library, 3.3 edition, Sweden, 2006.
[14] H. S. Won, K. C. Kim, S. H. Song, C. H. Oh, P. S. Kim, S. Park, and S. I. Kim, Appl. Phys. Lett. **88**, 011110 (2006).
[15] A. W. Snyder and J. D. Love, *Optical Waveguide Theory* (Chapman, London, 1983), pp. 212–214.
[16] T. Nakano, K. Baba, and M. Miyagi, J. Opt. Soc. Am. B **11**, 2030 (1994).
[17] P. S. Davids, B. A. Block, and K. C. Cadien, Opt. Express **13**, 7063 (2005).